Construction of a Retinal Atlas for Macular OCT Volumes

Arunava Chakravarty *, Divya Jyothi Gaddipati, Jayanthi Sivaswamy

Center for Visual Information Technology, KCIS, IIIT Hyderabad, India.
{arunava.chakravarty, divyajyothi.gaddipati}@research.iiit.ac.in,
jsivaswamy@iiit.ac.in

Abstract. Optical Coherence Tomography (OCT) plays an important role in the analysis of retinal diseases such as Age-Related Macular Degeneration (AMD). In this paper, we present a method to construct a normative atlas for macula centric OCT volumes with a mean intensity template (MT) and probabilistic maps for the seven intra-retinal tissue layers. We also propose an AMD classification scheme where the deviation of the local similarity of a test volume with respect to the MT is used to characterize AMD. The probabilistic atlas was used for layer segmentation where we achieved an average dice score of 0.82 across the eight layer boundaries. On the AMD detection task, the classification accuracy and Area under the Receiver Operating Characteristic curve were 98% and 0.996 respectively, on 170 OCT test volumes.

1 Introduction

Atlas plays an important role in medical image analysis by providing a standard coordinate frame to represent the anatomy. It is often in the form of a mean intensity template (MT) obtained by the average of a set of co-registered images along with a probability template (PT) which gives the probability of observing a particular structure at a given location. Normalization of images to a single coordinate frame via registration to the MT is useful in applications such as the segmentation of anatomical structures, disease detection and therapy planning.

Optical Coherence Tomography (OCT) has emerged as an important modality in retinal imaging by providing a high resolution 3D cross-sectional view of the intra-retinal tissue in a non-invasive manner. The intra-retinal tissue can be anatomically categorized into seven adjacent layers separated by eight boundaries [2] as depicted in Fig. 1 a. Quantitative measurements of the thickness and morphology of various layers are directly correlated to the health of the eye. For eg., in Age Related Macular Degenration (AMD), the drusen deposits occur in the Retinal Pigment Epithelium (RPE) layer leading to undulations in the Bruch's membrane (see Fig. 1 b.) around the macular region. The region between the ILM and Bruch's membrane is known as the Total Retina (TR) [3].

* This work is partially supported by Tata Consultancy Services (TCS) under their doctoral Research Scholarshp Program.

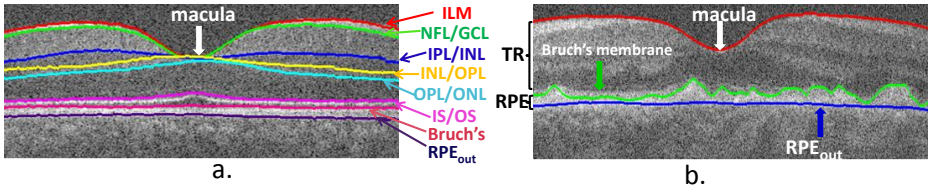

Fig. 1: a. A healthy OCT B-scan with eight layer boundaries. b. OCT B-scan of an AMD case with three relevant layer boundaries.

Though a Normative OCT atlas can have a wide range of applications in retinal image analysis including tissue layer segmentation, ocular disease detection and localization of abnormalities, its construction has received little attention. In [1], the similarity between pairs of A-scans was explored for the inter-subject registration of OCT volumes. The main challenges in the construction of an OCT atlas include the presence of speckle noise, vessel shadows and the inter or intra-scanner intensity variations across the A-scans. The curvature of the retinal surface also leads to large shifts in the retinal tissue across the B-scans.

The contribution of this paper is two-fold. (i) A Normative Atlas is constructed for the macular OCT volumes comprising a MT and the correspomding PT maps for seven retinal tissue layers.The OCT atlas is publicly available for research use at: https://researchweb.iiit.ac.in/~arunava.chakravarty/Atlas_mat_files.zip. (ii) The utility of the atlas is demonstrated through two applications, namely, the segmentation of intra-retinal tissue layers using label transfer and the detection of AMD in OCT volumes by leveraging the deviations in the local similarity between the MT and the registered test OCT Volumes.

2 Method

An overview of the atlas construction method is depicted in algorithm 1 and discussed in Section 2.1. The application of the atlas to layer segmentation and AMD detection (see Fig. 2) is detailed in Section 2.2. The preprocessing step comprises resizing, denoising, intensity standardization and retinal curvature flattening of the OCT volumes. Each B-scan in the OCT volume is resized to normalize the pixel dimensions to 3.6 μm by 8.6 μm. Denoising is done via speckle reducing anisotropic diffusion [15](30 iterations, timestep=0.1) and intensity standardization is achieved with a method reported in [9].

Retinal flattening is performed in two steps. First, each B-scan is individually flatenned using the method in [2] as follows. An approximate estimate of the outer RPE boundary is obtained by finding the brightest pixel in each A-scan, removing the outlier pixels and fitting a quadratic polynomial which is then mapped onto a straight line by shifting each column. In the second step, the B-scans are aligned across the volume. Each B-scan is sequentially aligned to its previous slice by an exhaustive search of the axial pixel translations that maximizes the normalized cross correlation (NCC) between them.

Algorithm 1: Atlas Construction

Input : Set of Normal OCT volumes $\{I_1, I_2 ... I_N\}$

Output: Atlas Mean Template $\mathcal{M}_T$

$\mathcal{M}_0 \leftarrow$ Select_Initial_Template$(I_1, I_2 ... I_N)$

for $t \leftarrow 1$ **to** T **do**

  $\hat{I}_i \leftarrow$Pairwise_Register $(I_i, \mathcal{M}_{t-1})$, $\forall 1 \leq i \leq N$

  $\mathcal{M}_t \leftarrow$Weighted_Average$(\hat{I}_1, ... \hat{I}_N)$

end

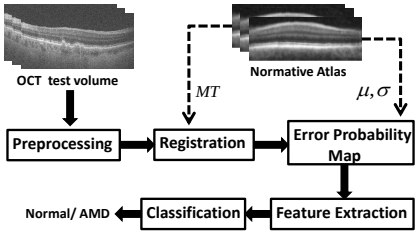

Fig. 2: AMD classification pipeline.

2.1 Atlas Construction

The construction of the atlas involves a groupwise registration of a set of preprocessed OCT volumes followed by computing their average to obtain the MT. A Sharp Means [14] based iterative method was adapted for this task. In each iteration (see algorithm 1), all OCT volumes are registered to the current mean intensity template $\mathcal{M}_{t-1}$ and their weighted average is used to update $\mathcal{M}_t$. The main challenge in the atlas construction is the large inter-subject variation which can result in a blurred $\mathcal{M}_t$, particularly in the initial iterations. To prevent blurring, the weights are adapted patchwise at each spatial location across each volume based on the local similarity between the registered volume $\hat{I}_i$ and $\mathcal{M}_{t-1}$ [14]. The final MT was obtained after $T = 10$ iterations and the patch size was decreased from $19 \times 19 \times 19$ to $1 \times 1 \times 1$ in steps of 2 at each iteration.

Our implementation differs from [14] in two ways: a) The initial template $\mathcal{M}_0$ is selected as the volume that lies closest to the geometric mean of the set using geodesic distance; b) Since size of the OCT volumes ($216 \times 770 \times 100$) is much larger than the typical size encountered in neuroimaging, we replace the Demon's registration approach in [14] with the discrete registration framework in [5] for the pairwise registrations to improve the computational efficiency.

The pairwise registration algorithm : The pairwise registration between a fixed (I_f) and moving (I_m) volume is performed in two steps. Since, registration along the axial direction is critical for the alignment of the anatomical layers, an initial rigid translation is performed along the axial direction by maximizing the global NCC of the entire volume using an exhaustive search of pixel translations. Next, a *symmetric* deformable registration is performed using a discrete optimization based method [5] which estimates the deformation field $\boldsymbol{u}$ as

$$\underset{\boldsymbol{u}}{\operatorname{argmin}}\, E(\boldsymbol{u}; I_f, I_m) = \sum_{p \in \Omega} S(I_f, I_m, \boldsymbol{u}_p) + \alpha . |\nabla \boldsymbol{u}|^2, \tag{1}$$

where p denotes each voxel location in the entire image domain Ω. NCC is chosen as the similarity function $S(I_f, I_m, \boldsymbol{u}_p)$ and computed between local patches centered around p. The deformable registration is performed at 3 scales. The maximum displacement was restricted to ± 7, ± 4 and ± 2 voxels from the coarse to fine scale respectively, along all the 3 axis. The regularization parameter σ

which indirectly controls the regularization weight α was set to 1 and the radius of local cost aggregation r was set to 2. (see [5] for more details).

Initial Template Selection : A method similar to [10], is used to select $\mathcal{M}_0$. Each OCT volume is represented as a node in a graph by constructing an adjacency matrix using the geodesic distance between each pair of volumes.

We define the geodesic distance between (I_i, I_j) as the registration error $E(\boldsymbol{u}^*; I_i, I_j)$ where $\boldsymbol{u}^*$ represents the displacement field obtained after registering I_j to I_i. In contrast, the bending energy of $\boldsymbol{u}^*$ alone was used in [10] to define the distance neglecting the similarity between the two image.

An adjacency matrix for the set of OCT volumes is constructed using the geodesic distance and Multidimensional Scaling (MDS) is applied to obtain a feature representation for each I_i such that the Euclidean distances in the feature space best approximates the corresponding geodesic distances in terms of the mean squared error [10]. Finally, the volume with the MDS feature closest to the mean feature of the entire set is selected as $\mathcal{M}_0$.

2.2 Applications

Our OCT atlas has the potential to become a useful resource in the field of retinal image analysis with various applications in layer segmentation, abnormality localization and ocular disease detection. In this work, we demonstrate its utility with two preliminary applications, the segmentation of intra-retinal tissue layers and the detection of AMD in OCT volumes.

OCT layer Segmentation

In order to use the atlas for intra-retinal tissue layer segmentation, the PT maps for the corresponding layers must be pre-computed during training. To compute the PT maps, a set of OCT volumes with manually segmented layers are employed. These OCT volumes are registered to the reference MT and its displacement field is applied to deform the corresponding groundtruth segmentation label maps. Finally, for each voxel in the atlas space, a probability value is computed for each label as the fraction of the registered volumes that have the label at that location.

During testing, a probabilistic segmentation is obtained by registering the atlas MT to a test OCT volume and applying the corresponding deformation field to the atlas PT maps for each layer. Further details on the datasets used in the PT map construction and it's performance are provided in Section 3.

AMD classification

The OCT atlas can aid in the detection of ocular diseases by enabling the extraction of a clinically relevant Region of Interest (ROI). Moreover, the higher registration errors for the abnormal images when registered to a Normative atlas can be leveraged to extract relevant features for disease classification.

We demonstrate this on the task of AMD detection. An atlas based approach has not been explored for AMD detection so far. Existing methods extract the RPE layer to define the (ROI) and employ handcrafted features such as Local Binary Patterns (LBP) [6], Histogram of Oriented Gradients (HoG) [11] or Bag

of visual words (BoW) [13] to detect AMD. The local features are aggregated using histogram [13] and employ multi-scale [11] or spatial pyramid [6] approaches to encode the spatial context. The details of the proposed atlas based method are outlined in Fig. 2 and described below.

ROI Extraction : A test OCT volume is first preprocessed and registered to the MT to obtain I_{tst}. Since the morphological changes in AMD are found in the area surrounding the macula in the RPE layer, a ROI is extracted in the atlas space for computational efficiency. The ROI is defined to span 31 B-scans and 180 A-scans centered at the macula. In the axial direction, the ROI is restricted to a small region around the *RPE* layer (rows 124-210 in the atlas space).

Error Probability Map Extraction : A local similarity measure for I_{tst} is evaluated at each voxel p within the ROI by extracting a $3 \times 3 \times 3$ patch $I_{tst}(p)$ around p and computing the NCC similarity $S(I_{tst}(p))$ with respect to the corresponding patch in the MT. The AMD cases (volumes) are expected to have smaller values for $S(I_{tst}(p))$ within the ROI.

However, the absolute value of the $S(I_{tst}(p))$ may not be meaningful. Depending on the complexity of the anatomical structure at a voxel location, the distribution of the local similarity of the Normal OCT volumes also varies across p. Hence the $S(I_{tst}(p))$ values are used to derive an error probability map $P_{err}(I_{tst})$. The $P_{err}(I_{tst})$ at location p measures the probability that $S(I_{tst}(p))$ is sampled from the distribution of similarity values at p that is encountered in the Normal OCT volumes. Assuming a Gaussian distribution for the similarity at each p independently, a mean ($\mu(p)$) and standard deviation $\sigma(p)$ map is generated for the ROI from the Normal OCT volumes used in the atlas construction. During testing, $P_{err}(I_{tst})$ is computed as $\frac{1}{\sqrt{2\pi\sigma(p)^2}} exp\{\frac{(S(I_{tst}(p))-\mu(p)).^2}{2\sigma(p)^2}\}$.

Feature Extraction and Classification : To obtain a global feature representation from the P_{err}, it is scaled to $[0, 1]$ across the samples. Thereafter, a 10 bin (uniform bins of width 0.1,centered at 0.05 to 0.95) histogram is computed. Though the abnormality can occur at any column position in the ROI, it should lie close to the bruch's membrane. Hence, the spatial location of the error probabilities along the rows may be important for classification. To incorporate this information, the ROI was further sub-divided into 6 equal row-wise sections and a separate histogram of the P_{err} was also computed for each sub-region. Finally, all histogram features were concatenated resulting in a $(10 + 10 \times 6 =)$70-D feature. A binary linear SVM classifier was employed for AMD classifcation.

3 Results

Dataset: The proposed method was evaluated using 290 (102 Normal, 188 AMD cases) 3D macular OCT volumes from a public dataset released in [3], henceforth referred to as the DUKE-3D dataset. The volumes were acquired from 4 clinics at a size of $512 \times 1000 \times 100$ with a voxel resolution of $(3.25, 6.7, 67)$ $\mu m/voxel$ along the axial, lateral and azimuthal directions. However, the ground truth(GT)

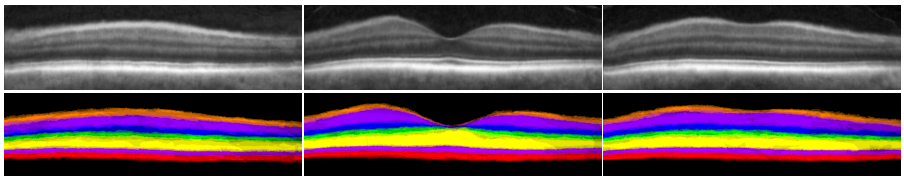

Fig. 3: (left to right) the mean intensity atlas (1^st row) and the corresponding probability maps for the seven tissue layers for the 30^{th}, 50^{th} and 60^{th} B-scans.

segmentation for only the RPE and TR tissue regions are provided in DUKE-3D. Therefore, two additional public datasets, OCTRIMA [12] and the dataset released in [2] (henceforth referred to as the DUKE-2D dataset) were employed to compute and evaluate the PT maps for the inner layers within the TR region (See Fig 1). Both OCTRIMA and DUKE-2D contain 10 OCT volumes each, acquired using different OCT scanners at varying resolutions (See [2], [12] for details). The two datasets provide the GT markings of seven retinal layers for only a few non-consecutive linearly spaced B-scans per volume (10 B-scans per volume in DUKE-2D and 11 B-scans per volume in OCTRIMA).

Intra-retinal layer segmentation The MT and PT maps for the TR and RPE regions were computed using 40 Normal OCT volumes and evaluated on the remaining (102-40) 62 Normal volumes in the DUKE-3D dataset. After thresholding the probabilities at 0.5, a mean dice score of 0.91 ± 0.02 and $\pm 0.78/0.06$ was achieved for the TR and RPE regions respectively.

To evaluate the localization of the inner layers, the PT maps were computed using the DUKE-2D dataset. Since, GT for only a few B-scans are available, the PT maps for each B-scan in the atlas was computed individually by registering to it, the nearest B-scan (with respect to the distance from macula) from each volume in DUKE-2D. The PT maps for the seven tissue layers are depicted in Fig. 3. The localization of all the seven layers were evaluated on the OCTRIMA dataset and benchmarked against three open source OCT segmentation softwares, the Iowa Reference Algorithm (IRA) version 3.8.0 based on [4], CASEREL based on [2] and OCTSEG based on [7]. CASEREL provides segmentation of seven boundaries (except the bruch's membrane) and OCTSEG segments six boundaries (except the bruch's membrane and INL/OPL). The quantitative results in Table 1 show our performance to be comparable to the existing methods. The probabilistic segmentation can also be used to provide a good initialization to deformable models such as [8] to further fine-tune the layer segmentation.

AMD classification The μ and σ used to compute the P_{err} was computed from the the 40 volumes from DUKE-3D used in the atlas construction. These volumes were excluded and the remaining OCT volumes in DUKE-3D were randomly divided into a separate training and test set consisting of 80 (22 Normal and 58 AMD cases) and 170(40 Normal and 130 AMD cases) respectively. The cost paramter of the linear SVM classifier set to 100 and the mis-classification penalty for each class was weighted during training to handle the class imbalance.

	NFL	GCL-IPL	INL	OPL	ONL-IS	OS	RPE
Dice							
CASEREL	0.81±0.13	0.78±0.11	0.50±0.14	0.62±0.12	0.90±0.06	—	—
OCTSEG	0.77±0.18	0.76±0.22	—	—	0.91±0.06	—	—
IRA	0.60±0.15	0.61±0.12	0.45±0.11	0.64±0.10	0.92±0.03	0.88±0.05	0.91±0.04
Proposed	0.79±0.08	0.89±0.07	0.81±0.07	0.75±0.08	0.93±0.03	0.74±0.11	0.83±0.06

Table 1: Dice coefficients (mean ± standard deviation) for the segmentation of 7 retinal tissue layers on the OCTRIMA dataset.

The classification performance is depicted in Table 2 and the corresponding ROC plot in Fig. 4. The good performance of our method with a linear classifier demonstrates the discriminative power of the proposed feature. Our atlas based feature outperforms the existing Bag of Words, multiscale HoG (MS-HoG) and the pyramid based SP-LBP features explored in [13], [11] and [6] respectively. [3] employed a manual segmentation of layer boundaries for AMD classification.

4 Conclusion

In this paper, we have constructed an atlas for normal OCT volumes which can be used in many applications such as extraction a clinically relevant ROI for analysis, characterize abnormalities as deviations from the Normative atlas or to provide intra-retinal tissue layer segmentations. The probabilistic segmentation maps of seven retinal tissue regions have been obtained which can be transferred onto the test images by registering them to the atlas MT. It achieved an average dice of 0.82 across the seven layers. Better registration algorithms specifically adapted for OCT volumes can be investigated in the future to further improve on the segmentation performance. We have also proposed a novel classification scheme for AMD which demonstrates state of the art performance with an accuracy of 98% and area under the ROC curve of 0.996 on a test set of 170 OCT volumes. Future work would investigate the characterization of additional pathologies such as cysts in the atlas space that appears in the TR region.

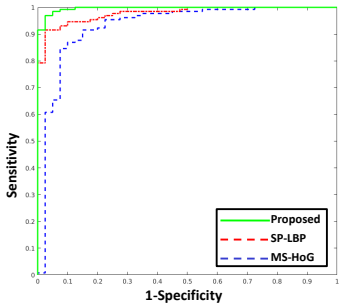

Fig. 4: ROC for AMD detection.

	Sens.	Spes.	Acc.	AUC
MS-HoG [11]	0.90	0.85	0.90	0.930
SP-LBP [6]	0.93	0.92	0.92	0.978
BoW [13]	0.96	0.92	0.94	0.984
Manual Seg. [3]	–	–	–	0.992
Proposed	0.97	0.98	0.98	0.996

Table 2: AMD classification performance.

References

1. Chen, M., Lang, A., Sotirchos, E., Ying, H.S., Calabresi, P.A., Prince, J.L., Carass, A.: Deformable registration of macular oct using a-mode scan similarity. In: IEEE International Symposium on Biomedical Imaging. pp. 476–479 (2013)
2. Chiu, S.J., Li, X.T., Nicholas, P., Toth, C.A., Izatt, J.A., Farsiu, S.: Automatic segmentation of seven retinal layers in sdoct images congruent with expert manual segmentation. Optics Express 18(18), 19413–19428 (2010)
3. Farsiu, S., Chiu, S.J., O'Connell, R.V., Folgar, F.A., Yuan, E., Izatt, J.A., Toth, C.A., et al.: Quantitative classification of eyes with and without intermediate age-related macular degeneration using optical coherence tomography. Ophthalmology 121(1), 162–172 (2014)
4. Garvin, M.K., Abràmoff, M.D., Wu, X., Russell, S.R., Burns, T.L., Sonka, M.: Automated 3-d intraretinal layer segmentation of macular spectral-domain optical coherence tomography images. IEEE Transactions on Medical Imaging 28(9), 1436–1447 (2009)
5. Heinrich, M.P., Papież, B.W., Schnabel, J.A., Handels, H.: Non-parametric discrete registration with convex optimisation. In: International Workshop on Biomedical Image Registration. pp. 51–61 (2014)
6. Liu, Y.Y., Chen, M., Ishikawa, H., Wollstein, G., Schuman, J.S., Rehg, J.M.: Automated macular pathology diagnosis in retinal oct images using multi-scale spatial pyramid and local binary patterns in texture and shape encoding. Medical Image Analysis 15(5), 748–759 (2011)
7. Mayer, M.A., Hornegger, J., Mardin, C.Y., Tornow, R.P.: Retinal nerve fiber layer segmentation on fd-oct scans of normal subjects and glaucoma patients. Biomedical Optics Express 1(5), 1358–1383 (2010)
8. Novosel, J., Thepass, G., Lemij, H.G., de Boer, J.F., Vermeer, K.A., van Vliet, L.J.: Loosely coupled level sets for simultaneous 3d retinal layer segmentation in optical coherence tomography. Medical Image Analysis 26(1), 146–158 (2015)
9. Nyúl, L.G., Udupa, J.K., Zhang, X.: New variants of a method of mri scale standardization. IEEE Transactions on Medical Imaging 19(2), 143–150 (2000)
10. Park, H., Bland, P.H., Hero, A.O., Meyer, C.R.: Least biased target selection in probabilistic atlas construction. In: International Conference on Medical Image Computing and Computer-Assisted Intervention. pp. 419–426 (2005)
11. Srinivasan, P.P., Kim, L.A., Mettu, P.S., Cousins, S.W., Comer, G.M., Izatt, J.A., Farsiu, S.: Fully automated detection of diabetic macular edema and dry age-related macular degeneration from optical coherence tomography images. Biomedical Optics Express 5(10), 3568–3577 (2014)
12. Tian, J., Varga, B., Somfai, G.M., Lee, W.H., Smiddy, W.E., DeBuc, D.C.: Real-time automatic segmentation of optical coherence tomography volume data of the macular region. PloS One 10(8), e0133908 (2015)
13. Venhuizen, F.G., van Ginneken, B., Bloemen, B., van Grinsven, M.J., Philipsen, R., Hoyng, C., Theelen, T., Sánchez, C.I.: Automated age-related macular degeneration classification in oct using unsupervised feature learning. In: SPIE Medical Imaging. pp. 94141I–94141I (2015)
14. Wu, G., Jia, H., Wang, Q., Shen, D.: Sharpmean: Groupwise registration guided by sharp mean image and tree-based registration. NeuroImage 56(4), 1968–1981 (2011)
15. Yu, Y., Acton, S.T.: Speckle reducing anisotropic diffusion. IEEE Transactions on Image Processing 11(11), 1260–1270 (2002)